Monthly Notices
of the
ROYAL ASTRONOMICAL SOCIETY

Mon. Not. R. Astron. Soc. **410,** 2730–2740 (2011) doi:10.1111/j.1365-2966.2010.17638.x

Tidal alignments as a contaminant of the galaxy bispectrum

Elisabeth Krause[1⋆] and Christopher M. Hirata[2]

[1]*Caltech M/C 249-17, Pasadena, CA 91125, USA*
[2]*Caltech M/C 350-17, Pasadena, CA 91125, USA*

Accepted 2010 September 5. Received 2010 August 31; in original form 2010 April 20

ABSTRACT

If the orientations of galaxies are correlated with large-scale structure, then anisotropic selection effects such as preferential selection of face-on disc galaxies can contaminate large-scale structure observables. Here we consider the effect on the galaxy bispectrum, which has attracted interest as a way to break the degeneracy between galaxy bias and the amplitude of matter fluctuations σ_8. We consider two models of intrinsic galaxy alignments: one where the probability distribution for the galaxy's orientation contains a term linear in the local tidal field, appropriate for elliptical galaxies; and one with a term quadratic in the local tidal field, which may be applicable to disc galaxies. We compute the correction to the redshift space bispectrum in the quasi-linear regime, and then focus on its effects on parameter constraints from the transverse bispectrum, i.e. using triangles $(\boldsymbol{k}_1, \boldsymbol{k}_2, \boldsymbol{k}_3)$ in the plane of the sky. We show that in the linear alignment model, intrinsic alignments result in an error in the galaxy bias parameters, but do not affect the inferred value of σ_8. In contrast, the quadratic alignment model results in a systematic error in both the bias parameters and σ_8. However, the quadratic alignment effect has a unique configuration dependence that should enable it to be removed in upcoming surveys.

Key words: cosmology: theory – large-scale structure of Universe.

1 INTRODUCTION

While the evolution of dark matter perturbations in the current ΛCDM model is well understood theoretically, the relation between the galaxy distribution and the large-scale (dark) matter distribution is complicated by the detailed physics of galaxy formation and different models may lead to different clustering properties of galaxies. In particular, while local theories of galaxy formation predict that the galaxy density fluctuations trace the matter fluctuations on large scales, they also predict that the two are related by the *bias parameter b*, which is in general not known a priori (Kaiser 1984). The unknown bias parameter represents a key problem for attempts to measure the growth of cosmological perturbations using galaxies.

In combination with the galaxy power spectrum, third-order galaxy clustering measures such as the bispectrum or (equivalently) the three-point correlation function can be used to measure non-linear galaxy bias and break the degeneracy between the normalization of the matter power spectrum, σ_8, and the linear galaxy bias. This enables one to remove the effects of galaxy biasing and measure the cosmological growth of structure from the galaxy distribution (Fry 1994; Verde et al. 1998; Scoccimarro, Couchman & Frieman 1999; Verde, Heavens & Matarrese 2000), and thus constrain dark energy (e.g. Dolney, Jain & Takada 2006). Recently third-order galaxy clustering has been analyzed by several authors using the bispectrum (Feldman et al. 2001; Scoccimarro et al. 2001; Verde et al. 2002; Kulkarni et al. 2007) and the three-point correlation function (Jing & Börner 2004; Kayo et al. 2004; Nichol et al. 2006). Using mock catalogues from numerical simulations, Sefusatti et al. (2006) show that a combined analysis of the galaxy power spectrum and bispectrum including their cross-correlation contains significant information on galaxy bias and fundamental cosmological parameters and helps break parameter degeneracies of other cosmological probes.

The most important systematic errors in interpreting the observed galaxy clustering arise in the non-linear regime, where the behaviour of galaxy biasing and models of the (redshift space) galaxy power spectrum and bispectrum are difficult to model (see Smith, Sheth & Scoccimarro 2008, for the complications of a current model of the redshift space bispectrum). Recently Hirata (2009) showed that the alignment of galaxies by large-scale tidal fields can cause a systematic error in the determination of the linear redshift space distortion parameter β (Kaiser 1987): the alignment of galaxies with the tidal field (along the stretching axis of the field for large elliptical galaxies) in combination with a viewing-direction-dependent galaxy-selection effect, e.g. preferential selection of galaxies which are observed along their long axis, will lead to a selection probability for galaxies which is modulated by the tidal field along the line of sight. This results in an anisotropy in redshift space clustering with the same scale and angular dependence as the linear redshift

⋆E-mail: ekrause@astro.caltech.edu

space effect. In this paper we will explore the implications of such a tidal alignment contamination for the observed galaxy bispectrum and how it affects the measurement of galaxy bias parameters.

Throughout this paper we assume a standard ΛCDM cosmology with the best-fitting *WMAP* 7 (Komatsu et al. 2010) parameters, and assume Gaussian initial density perturbations.

We begin in Section 2 with a derivation of the standard redshift space galaxy bispectrum and discuss toy models for physical processes that cause alignments of galaxy orientations with large-scale structure. In Section 3 we explain how tidal alignments of galaxies in combination with an orientation-dependent galaxy selection modify the observed galaxy distribution and calculate the corresponding corrections to the galaxy bispectrum. Using a Fisher matrix technique we then estimate the systematic error induced by tidal alignments to measurements of galaxy bias parameters from angular clustering in Section 4. We conclude and discuss mitigation strategies in Section 5.

2 THEORETICAL BACKGROUND

In this section we derive the redshift space galaxy bispectrum to second order in perturbation theory (for a review, see e.g. Bernardeau et al. 2002), and discuss toy models for the alignment of galaxies with the large-scale tidal field.

2.1 Galaxy bispectrum

The matter bispectrum B is defined as

$$\langle\tilde{\delta}(\boldsymbol{k}_1)\tilde{\delta}(\boldsymbol{k}_2)\tilde{\delta}(\boldsymbol{k}_3)\rangle \equiv (2\pi)^3\delta_{\rm D}\left(\boldsymbol{k}_{123}\right)B(\boldsymbol{k}_1,\boldsymbol{k}_2,\boldsymbol{k}_3), \tag{1}$$

where $\tilde{\delta}(\boldsymbol{k})$ is the matter density contrast in Fourier space, $\delta_{\rm D}$ the Dirac delta function and $\boldsymbol{k}_{123} \equiv \boldsymbol{k}_1+\boldsymbol{k}_2+\boldsymbol{k}_3$. The bispectrum vanishes for a Gaussian random field.

To second-order perturbation theory the density contrast is given by

$$\tilde{\delta}(\boldsymbol{k}) = \tilde{\delta}^{(1)}(\boldsymbol{k}) + \int\frac{{\rm d}^3\boldsymbol{k}_1}{(2\pi)^3}F_2\left(\boldsymbol{k}_1,\boldsymbol{k}-\boldsymbol{k}_1\right)\tilde{\delta}^{(1)}(\boldsymbol{k}_1)\tilde{\delta}^{(1)}(\boldsymbol{k}-\boldsymbol{k}_1), \tag{2}$$

with $\tilde{\delta}^{(1)}(\boldsymbol{k})$ being the linear density contrast, and the second-order density kernel

$$F_2(\boldsymbol{k}_1,\boldsymbol{k}_2) = \frac{5}{7} + \frac{\boldsymbol{k}_1\cdot\boldsymbol{k}_2}{2k_1k_2}\left(\frac{k_1}{k_2}+\frac{k_2}{k_1}\right) + \frac{2}{7}\left(\frac{\boldsymbol{k}_1\cdot\boldsymbol{k}_2}{k_1k_2}\right)^2. \tag{3}$$

Hence the matter bispectrum induced by non-linear gravitational evolution at tree-level is given by

$$B(\boldsymbol{k}_1,\boldsymbol{k}_2,\boldsymbol{k}_3) = 2F_2(\boldsymbol{k}_1,\boldsymbol{k}_2)P(k_1)P(k_2) + 2\ \text{perm.}, \tag{4}$$

where $P(k)$ is the linear matter power spectrum, $\boldsymbol{k}_3 = -\boldsymbol{k}_1-\boldsymbol{k}_2$ and '2 perm.' indicates that the two permutations $(\boldsymbol{k}_2,\boldsymbol{k}_3)$ and $(\boldsymbol{k}_1,\boldsymbol{k}_3)$ are also included in the summation.

Using the local bias approximation (e.g. Fry & Gaztañaga 1993), the galaxy density contrast $\delta_{\rm g}$ can be expressed as a non-linear function of the matter density contrast

$$\delta_{\rm g}(\boldsymbol{x}) = b_1\delta(\boldsymbol{x}) + \frac{1}{2}b_2\delta(\boldsymbol{x})^2 + \cdots, \tag{5}$$

where the expansion coefficients are the linear (b_1) and non-linear galaxy bias factors. In reality, galaxy biasing may be more complicated, especially on small scales, due to one-halo terms (Seljak 2000) and non-local dependences such as the strength of the local tidal field (McDonald 2006; McDonald & Roy 2009). However, in simulations the local bias model is found to be a fair description of non-linear halo clustering on large scales with an accuracy of a few per cent (e.g. Marín et al. 2008; Guo & Jing 2009b; Manera & Gaztañaga 2009), which is sufficient at the level of this analysis.

Then the galaxy bispectrum $B_{\rm g}$ is related to the matter bispectrum via

$$B_{\rm g}(\boldsymbol{k}_1,\boldsymbol{k}_2,\boldsymbol{k}_3) \simeq b_1^3B(\boldsymbol{k}_1,\boldsymbol{k}_2,\boldsymbol{k}_3) + b_1^2b_2[P(k_1)P(k_2)+2\ \text{perm.}], \tag{6}$$

and similarly for the galaxy power spectrum,

$$P_{\rm g}(k) = b_1^2P(k). \tag{7}$$

To arrive at an expression for the redshift space galaxy bispectrum we have to transform radial coordinates to redshift space. In the plane-parallel approximation, the mapping from the real-space position $\boldsymbol{x}$ to the coordinate $\boldsymbol{x}^{\rm s}$ in redshift space is given by

$$\boldsymbol{x}^{\rm s} = \boldsymbol{x} + \frac{\hat{\boldsymbol{n}}\cdot\boldsymbol{u}(\boldsymbol{x})}{Ha}\hat{\boldsymbol{n}}, \tag{8}$$

where $\boldsymbol{u}(\boldsymbol{x})$ is the peculiar velocity field and $\hat{\boldsymbol{n}}$ is the direction of the line of sight. The velocity field is curl-free, $\nabla\times\boldsymbol{u}(\boldsymbol{x}) = 0$, at all orders in perturbation theory. Its divergence is given to linear order in perturbation theory by

$${\rm i}\boldsymbol{k}\cdot\tilde{\boldsymbol{u}}^{(1)}(\boldsymbol{k}) = aHf\tilde{\delta}^{(1)}(\boldsymbol{k}), \tag{9}$$

where $f = {\rm d}\ln(G)/{\rm d}\ln(a)$ is the logarithmic growth rate of linear perturbations (equal to roughly $\Omega_{\rm m}^{0.6}$ in general relativity). Higher-order contributions to $\nabla\cdot\boldsymbol{u}$ (Bernardeau et al. 2002) are analogous to equation (2), e.g.

$${\rm i}\boldsymbol{k}\cdot\tilde{\boldsymbol{u}}^{(2)}(\boldsymbol{k}) = aHf\int\frac{{\rm d}^3\boldsymbol{k}_1}{(2\pi)^3}G_2(\boldsymbol{k}_1,\boldsymbol{k}-\boldsymbol{k}_1)\tilde{\delta}^{(1)}(\boldsymbol{k}_1)\tilde{\delta}^{(1)}(\boldsymbol{k}-\boldsymbol{k}_1), \tag{10}$$

with the kernel

$$G_2(\boldsymbol{k}_1,\boldsymbol{k}_2) = \frac{3}{7} + \frac{\boldsymbol{k}_1\cdot\boldsymbol{k}_2}{2k_1k_2}\left(\frac{k_1}{k_2}+\frac{k_2}{k_1}\right) + \frac{4}{7}\left(\frac{\boldsymbol{k}_1\cdot\boldsymbol{k}_2}{k_1k_2}\right)^2. \tag{11}$$

Taking into account the Jacobian of this mapping of $\boldsymbol{x}\rightarrow\boldsymbol{x}^{\rm s}$ (equation (8)), and approximating the peculiar velocity field by the second-order bulk velocity field, the galaxy density in redshift space is (Heavens, Matarrese & Verde 1998; Scoccimarro et al. 1999)

$$\tilde{\delta}_{\rm g}^{\rm s}(\boldsymbol{k}^{\rm s}) = (b_1+f\mu^2)\tilde{\delta}^{(1)}(\boldsymbol{k}^{\rm s}) + \int\frac{{\rm d}^3\boldsymbol{k}_1^{\rm s}}{(2\pi)^3}Z_2\left(\boldsymbol{k}_1^{\rm s},\boldsymbol{k}^{\rm s}-\boldsymbol{k}_1^{\rm s}\right)\tilde{\delta}^{(1)}\left(\boldsymbol{k}_1^{\rm s}\right)\tilde{\delta}^{(1)}\left(\boldsymbol{k}^{\rm s}-\boldsymbol{k}_1^{\rm s}\right), \tag{12}$$

where $\boldsymbol{k}^{\rm s}$ denotes a Fourier mode in redshift space and $\mu\equiv\hat{\boldsymbol{k}}\cdot\hat{\boldsymbol{n}}$ is the cosine of the angle between the wave vector and the line of sight (we may analogously define μ_1,μ_{12}, etc.). The mode-coupling function Z_2 is

$$Z_2(\boldsymbol{k}_1,\boldsymbol{k}_2) = b_1F_2(\boldsymbol{k}_1,\boldsymbol{k}_2) + f\mu_{12}^2G_2(\boldsymbol{k}_1,\boldsymbol{k}_2) + \frac{f\mu_{12}k_{12}}{2}\left[\frac{\mu_1}{k_1}\left(b_1+f\mu_2^2\right)+\frac{\mu_2}{k_2}\left(b_1+f\mu_1^2\right)\right] + \frac{b_2}{2}, \tag{13}$$

Hence we can write the redshift space galaxy bispectrum as

$$B_{\rm g}^{\rm s}\left(\boldsymbol{k}_1^{\rm s},\boldsymbol{k}_2^{\rm s},\boldsymbol{k}_3^{\rm s}\right) = 2\left(b_1+f\mu_1^2\right)\left(b_1+f\mu_2^2\right)P\left(k_1^{\rm s}\right)P\left(k_2^{\rm s}\right)Z_2\left(\boldsymbol{k}_1^{\rm s},\boldsymbol{k}_2^{\rm s}\right) + 2\,\text{perm.} \tag{14}$$

Note that this expression does not include the *Finger of God* effect due to the virialized motion of galaxies within a cluster (Jackson 1972), which is important when one of the k_i has a large line-of-sight component. While this effect is important even on weakly non-linear scales, it is usually handled by phenomenological models (e.g. Hatton & Cole 1998; Verde et al. 1998; Scoccimarro et al. 1999; Peacock et al. 2001), a compression of radial coordinates for galaxies living in the same cluster (e.g. Tegmark et al. 2004), or by reconstructing the redshift space halo density field (Reid, Spergel & Bode 2009).

2.2 Toy models of tidal alignments

2.2.1 Halo shape distortions: linear alignment

In the linear alignment model (Catelan, Kamionkowski & Blandford 2001) the shape and orientation of a galaxy are assumed to be determined by the shape of the halo it resides in. It is thought that the gravitational collapse of an initially spherical overdensity in a constant gravitational field leads to triaxial haloes, such that the halo will be prolate if the overdensity is stretched by the large-scale tidal field and oblate if it is compressed. This mechanism is believed to lead to a net correlation of halo orientations even though overdensities typically are not spherical, and such an alignment has been confirmed by simulations (e.g. Faltenbacher et al. 2009).

The relation between halo shape and galaxy shape is complicated by galaxy formation and differs between galaxy types (e.g. Faltenbacher et al. 2007), but at least for luminous red galaxies (LRGs) there is observational evidence for an alignment of the LRG with the major axis of its host (Binggeli 1982; Faltenbacher et al. 2007; Niederste-Ostholt et al. 2010). There are also correlations with large-scale structure (Binggeli 1982); with the Sloan Digital Sky Survey (SDSS) it has even been possible to measure the scale dependence of these correlations and show the consistency of their spectral index with the predictions of the linear tidal alignment model and the ΛCDM power spectrum (Hirata et al. 2007).

2.2.2 Tidal torques: quadratic alignment

The orientation of a disc galaxy is determined by the direction of its angular momentum, which builds up due to tidal torquing during early stages of galaxy formation if the proto-galaxy's inertia tensor is anisotropic and misaligned with the local shear field (Hoyle 1949; Sciama 1955; Peebles 1969; Doroshkevich 1970; White 1984; Crittenden et al. 2001). See Schäfer (2009) for a review of tidal torquing and the build up of angular momentum correlations.

Following Lee & Pen (2000), we parametrize the correlation between moment of inertia and the shear field by

$$\langle L_i L_j \rangle = \langle L^2 \rangle \left(\frac{1+\alpha}{3} \delta_{ij} - \alpha \hat{T}_{ih} \hat{T}_{hj} \right), \tag{15}$$

which is also the most general quadratic form possible. Here $\hat{T}_{ij}$ is the unit normalized traceless tidal field tensor ($\hat{T}_{ij}\hat{T}_{ij} = 1$) and α is a dimensionless coupling parameter, e.g. $\alpha = \frac{3}{5}$ at leading order in perturbation theory if shear and inertia tensor are mutually uncorrelated. It is also possible for α to be much smaller, e.g. if the angular momentum vector of the disc is only partially aligned with that of the host halo (e.g. van den Bosch et al. 2002).

Note that in non-linear theory spin-induced alignments also have a linear contribution at large scales because the large-scale tidal field induces correlations of the small-scale tidal field and inertia tensor that lead to a non-zero contribution to $\langle L_i L_j \rangle$ (Hui & Zhang 2008), although this linear effect has not been observed for late-type galaxies despite several searches (Hirata et al. 2007; Lee & Pen 2007; Mandelbaum et al. 2009).

3 TIDAL ALIGNMENT CONTAMINATION

As discussed in the previous section, the orientation of galaxies likely is not random but correlated with large-scale structure, and in combination with observational galaxy selection criteria which depend on the galaxy orientation relative to the line of sight, this may modify the observable galaxy distribution. Following Hirata (2009), we will now introduce the basic notation needed to discuss galaxy orientation- and viewing-direction-dependent selection effects.

Let the galaxy orientation be described by the Euler angles (θ, ϕ, ψ) through a rotation matrix $\mathbf{Q}(\theta, \phi, \psi)$. This matrix transforms 'lab' frame coordinates to a coordinate system aligned with the galaxy. Due to tidal alignments the probability distribution $p(\mathbf{Q}|\boldsymbol{x})$ for the orientation of a galaxy at position $\boldsymbol{x}$ may be anisotropic and a function of the local environment of $\boldsymbol{x}$. The observational galaxy selection probability depends on the direction of the line of sight, $\hat{\boldsymbol{n}}$, and the galaxy orientation, specifically on the direction of the line of sight in the galaxy frame $\mathbf{Q}\hat{\boldsymbol{n}}$. We define

$$P \propto 1 + \Upsilon\left(\mathbf{Q}\hat{\boldsymbol{n}}, \boldsymbol{x}\right), \tag{16}$$

where the anisotropic part Υ is zero when averaged over all possible galaxy orientations or viewing directions.

The observable galaxy distribution N (selected) hence is modified compared to the true galaxy distribution N(true) by

$$\begin{aligned} \frac{N(\text{selected})}{N(\text{true})}(\hat{\boldsymbol{n}}|\boldsymbol{x}) &\propto \int_{\mathrm{SO}(3)} p(\mathbf{Q}|\boldsymbol{x}) \left[1 + \Upsilon\left(\mathbf{Q}\hat{\boldsymbol{n}}, \boldsymbol{x}\right)\right] \, \mathrm{d}^3\mathbf{Q} \\ &= 1 + \int_{\mathrm{SO}(3)} p(\mathbf{Q}|\boldsymbol{x}) \Upsilon\left(\mathbf{Q}\hat{\boldsymbol{n}}, \boldsymbol{x}\right) \, \mathrm{d}^3\mathbf{Q} \\ &\equiv 1 + \epsilon(\hat{\boldsymbol{n}}|\boldsymbol{x}), \end{aligned} \tag{17}$$

which is the average of equation (16) over the distribution of galaxy orientations, and where we have defined the orientation-dependent selection function $\epsilon(\hat{\boldsymbol{n}}|\boldsymbol{x})$ in the last step. As the average of Υ over all galaxy orientations vanishes, equation (17) implies that ϵ vanishes if either the galaxy orientations are isotropically distributed or if the probability for selecting a galaxy is independent of $\mathbf{Q}\hat{\boldsymbol{n}}$, i.e. if $\Upsilon = 0$.

The observed galaxy density is modified by the orientation-dependent selection function such that

$$1 + \delta_{\mathrm{g}}^{\mathrm{obs}}(\boldsymbol{x}^{\mathrm{s}}) = \{[1 + \delta_{\mathrm{g}}(\boldsymbol{x})][1 + \epsilon(\hat{\boldsymbol{n}}|\boldsymbol{x})]\}^{\mathrm{s}}, \tag{18}$$

where the term in curly brackets is the orientation-modulated real space density of selected galaxies, and where the superscript s denotes the transformation to redshift space. Expanding to second order in the matter density field, this implies

$$\begin{aligned} \tilde{\delta}_{\mathrm{g}}^{\mathrm{obs}}(\boldsymbol{k}^{\mathrm{s}}) = \tilde{\delta}_{\mathrm{g}}^{\mathrm{s}(1)}(\boldsymbol{k}^{\mathrm{s}}) + \tilde{\epsilon}^{\mathrm{s}(1)}(\hat{\boldsymbol{n}}|\boldsymbol{k}^{\mathrm{s}}) + \tilde{\delta}_{\mathrm{g}}^{\mathrm{s}(2)}(\boldsymbol{k}^{\mathrm{s}}) + \tilde{\epsilon}^{\mathrm{s}(2)}(\hat{\boldsymbol{n}}|\boldsymbol{k}^{\mathrm{s}}) \\ + \int \frac{\mathrm{d}^3\boldsymbol{k}_1^{\mathrm{s}}}{(2\pi)^3} \tilde{\delta}_{\mathrm{g}}^{\mathrm{s}(1)}\left(\boldsymbol{k}_1^{\mathrm{s}}\right) \tilde{\epsilon}^{\mathrm{s}(1)}\left(\hat{\boldsymbol{n}}|\boldsymbol{k}^{\mathrm{s}} - \boldsymbol{k}_1^{\mathrm{s}}\right). \end{aligned} \tag{19}$$

In the following we calculate the impact of an orientation-dependent selection function on the galaxy bispectrum by introducing models for the anisotropic galaxy selection function which are based on symmetry considerations and motivated by the toy models of tidal alignment discussed in Section 3. First we extend the linear alignment model from Hirata (2009) to second order in the density field, and then construct a new model from the anisotropic galaxy selection function due to quadratic alignment.

3.1 Linear alignment

In this subsection we construct a model for the anisotropic galaxy selection function ϵ based on the assumptions that the large-scale tidal fields induce a preferred direction in galaxy formation, and that the alignment is of linear order in the tidal field. Additionally we require the average of $\epsilon(\hat{\boldsymbol{n}}|\boldsymbol{x})$ over the sky to vanish. Then the only possible contraction of the tidal field with the viewing direction $\hat{\boldsymbol{n}}$ is

$$\begin{aligned}\epsilon(\hat{\boldsymbol{n}}|\boldsymbol{x}) &= \frac{A_1}{4\pi G a^2 \bar{\rho}_{\rm m}(a)}\left(\hat{n}_i\hat{n}_j\nabla_i\nabla_j - \frac{1}{3}\nabla^2\right)\Psi(\boldsymbol{x}) \\ &= A_1\hat{n}_i\hat{n}_j\left(\nabla_i\nabla_j\nabla^{-2} - \frac{1}{3}\delta_{ij}\right)\delta(\boldsymbol{x}),\end{aligned} \tag{20}$$

where Ψ is the Newtonian potential, a is the scalefactor and where we have used the Poisson equation to write ϵ in terms of the dimensionless tidal field. A_1 is an expansion coefficient which encodes the degree to which galaxy orientations are non-random due to tidal fields and the strength of galaxy orientation-dependent selection effects. Note that *both* effects need to be present in order to have $A_1 \neq 0$.

To second order in the linear matter density field the anisotropic selection function in Fourier space can be written as

$$\tilde{\epsilon}(\hat{\boldsymbol{n}}|\boldsymbol{k}) \approx A_1\left[(\hat{\boldsymbol{n}}\cdot\hat{\boldsymbol{k}})^2 - \frac{1}{3}\right][\tilde{\delta}^{(1)}(\boldsymbol{k}) + \tilde{\delta}^{(2)}(\boldsymbol{k})]. \tag{21}$$

This expression is transformed to redshift space by Taylor expanding the real-space expression and using equations (8) and (9):

$$\begin{aligned}\epsilon^{\rm s}(\hat{\boldsymbol{n}}|\boldsymbol{x}^{\rm s}) &= \epsilon(\hat{\boldsymbol{n}}|\boldsymbol{x}) \approx \epsilon(\hat{\boldsymbol{n}}|\boldsymbol{x}^{\rm s}) + (\boldsymbol{x}-\boldsymbol{x}^{\rm s})\cdot\nabla\epsilon(\hat{\boldsymbol{n}}|\boldsymbol{x}^{\rm s}) + \mathcal{O}(\delta^3) \\ &= \epsilon(\hat{\boldsymbol{n}}|\boldsymbol{x}^{\rm s}) + f\hat{\boldsymbol{n}}\cdot\nabla\,\nabla^{-2}\delta^{(1)}(\boldsymbol{x}^{\rm s})\,\hat{\boldsymbol{n}}\cdot\nabla\epsilon(\hat{\boldsymbol{n}}|\boldsymbol{x}^{\rm s})\,,\end{aligned} \tag{22}$$

and hence in Fourier space,

$$\begin{aligned}\tilde{\epsilon}^{\rm s(1)}(\hat{\boldsymbol{n}}|\boldsymbol{k}^{\rm s}) &= \tilde{\epsilon}^{(1)}(\hat{\boldsymbol{n}}|\boldsymbol{k}^{\rm s}), \\ \tilde{\epsilon}^{\rm s(2)}(\hat{\boldsymbol{n}}|\boldsymbol{k}^{\rm s}) &= \tilde{\epsilon}^{(2)}(\hat{\boldsymbol{n}}|\boldsymbol{k}^{\rm s}) \\ &\quad + \int\frac{{\rm d}^3\boldsymbol{k}_1^{\rm s}}{(2\pi)^3}f\mu_1\mu_{\boldsymbol{k}^{\rm s}-\boldsymbol{k}_1^{\rm s}}\frac{k_1^{\rm s}}{|\boldsymbol{k}^{\rm s}-\boldsymbol{k}_1^{\rm s}|} \\ &\quad \times\tilde{\delta}^{(1)}\left(\boldsymbol{k}^{\rm s}-\boldsymbol{k}_1^{\rm s}\right)\tilde{\epsilon}^{(1)}\left(\hat{\boldsymbol{n}}|\boldsymbol{k}_1^{\rm s}\right).\end{aligned} \tag{23}$$

Using this form for the selection function in combination with equation (19), we now calculate the galaxy bispectrum modulated by linear tidal alignments. Then the first-order observed density contrast is given by:

$$\tilde{\delta}_{\rm g}^{\rm obs(1)}(\boldsymbol{k}^{\rm s}) = \tilde{\delta}^{(1)}(\boldsymbol{k})\left[b_1 - \frac{1}{3}A_1 + (A_1+f)\mu_1^2\right]\,. \tag{24}$$

The different terms contributing to the observed galaxy bispectrum can be calculated as

$$\begin{aligned}\left\langle\tilde{\delta}_{\rm g}^{\rm obs(1)}\left(\boldsymbol{k}_1^{\rm s}\right)\tilde{\delta}_{\rm g}^{\rm obs(1)}\left(\boldsymbol{k}_2^{\rm s}\right)\tilde{\delta}_{\rm g}^{\rm s(2)}\left(\boldsymbol{k}_3^{\rm s}\right)\right\rangle &= (2\pi)^3\delta_{\rm D}\left(\boldsymbol{k}_{123}^{\rm s}\right)P\left(k_1^{\rm s}\right)P\left(k_2^{\rm s}\right) \\ &\quad\times\left[b_1 - \frac{1}{3}A_1 + (A_1+f)\mu_1^2\right] \\ &\quad\times\left[b_1 - \frac{1}{3}A_1 + (A_1+f)\mu_2^2\right] \\ &\quad\times 2\,Z_2\left(\boldsymbol{k}_1^{\rm s},\boldsymbol{k}_2^{\rm s}\right)\,,\end{aligned} \tag{25}$$

$$\begin{aligned}\left\langle\tilde{\delta}_{\rm g}^{\rm obs(1)}\left(\boldsymbol{k}_1^{\rm s}\right)\tilde{\delta}_{\rm g}^{\rm obs(1)}\left(\boldsymbol{k}_2^{\rm s}\right)\tilde{\epsilon}^{\rm s(2)}\left(\hat{\boldsymbol{n}}|\boldsymbol{k}_3^{\rm s}\right)\right\rangle &= (2\pi)^3\delta_{\rm D}\left(\boldsymbol{k}_{123}^{\rm s}\right)P\left(k_1^{\rm s}\right)P\left(k_2^{\rm s}\right) \\ &\quad\times\left[b_1 - \frac{1}{3}A_1 + (A_1+f)\mu_1^2\right] \\ &\quad\times\left[b_1 - \frac{1}{3}A_1 + (A_1+f)\mu_2^2\right] \\ &\quad\times\left[2A_1\left(\mu_{12}^2 - \frac{1}{3}\right)F_2(\boldsymbol{k}_1,\boldsymbol{k}_2)\right. \\ &\quad + A_1 f\mu_1\mu_2\frac{k_1^{\rm s}}{k_2^{\rm s}}\left(\mu_1^2 - \frac{1}{3}\right) \\ &\quad\left. + A_1 f\mu_1\mu_2\frac{k_2^{\rm s}}{k_1^{\rm s}}\left(\mu_2^2 - \frac{1}{3}\right)\right]\end{aligned} \tag{26}$$

and the contribution from the last term in equation (19) containing a convolution of first-order density contrast and anisotropic selection function:

$$\begin{aligned}&\left\langle\tilde{\delta}_{\rm g}^{\rm obs(1)}\left(\boldsymbol{k}_1^{\rm s}\right)\tilde{\delta}_{\rm g}^{\rm obs(1)}\left(\boldsymbol{k}_2^{\rm s}\right)\left(\tilde{\delta}_{\rm g}^{\rm s(1)}\otimes\tilde{\epsilon}^{\rm s(1)}\right)\left(\hat{\boldsymbol{n}},\boldsymbol{k}_3^{\rm s}\right)\right\rangle \\ &\quad= (2\pi)^3\delta_{\rm D}\left(\boldsymbol{k}_{123}^{\rm s}\right)P\left(k_1^{\rm s}\right)P\left(k_2^{\rm s}\right) \\ &\qquad\times\left[b_1 - \frac{1}{3}A_1 + (A_1+f)\mu_1^2\right]\left[b_1 - \frac{1}{3}A_1 + (A_1+f)\mu_2^2\right] \\ &\qquad\times A_1\left[\left(b_1 + f\mu_1^2\right)\left(\mu_2 - \frac{1}{3}\right) + \left(b_1 + f\mu_2^2\right)\left(\mu_1 - \frac{1}{3}\right)\right].\end{aligned} \tag{27}$$

Hence the galaxy bispectrum modulated by linear tidal alignments is given by

$$\begin{aligned}B_{\rm g}^{\rm s,LA}\left(\boldsymbol{k}_1^{\rm s},\boldsymbol{k}_2^{\rm s},\boldsymbol{k}_3^{\rm s}\right) &= \left[b_1 - \frac{A_1}{3} + (A_1+f)\mu_1^2\right] \\ &\quad\times\left[b_1 - \frac{A_1}{3} + (A_1+f)\mu_2^2\right] \\ &\quad\times\left\{2Z_2\left(\boldsymbol{k}_1^{\rm s},\boldsymbol{k}_2^{\rm s}\right) + 2A_1\left(\mu_{12}^2 - \frac{1}{3}\right)F_2\left(\boldsymbol{k}_1^{\rm s},\boldsymbol{k}_2^{\rm s}\right)\right. \\ &\quad + A_1\left[b_1\left(\mu_1^2+\mu_2^2 - \frac{2}{3}\right)\right. \\ &\quad\left. + \frac{f}{3}\left(6\mu_1^2\mu_2^2 - \mu_1^2 - \mu_2^2\right)\right] \\ &\quad + A_1 f\mu_1\mu_2\left[\frac{k_2^{\rm s}}{k_1^{\rm s}}\left(\mu_2^2 - \frac{1}{3}\right)\right. \\ &\quad\left.\left. + \frac{k_1^{\rm s}}{k_2^{\rm s}}\left(\mu_1^2 - \frac{1}{3}\right)\right]\right\}P\left(k_1^{\rm s}\right)P\left(k_2^{\rm s}\right) + 2\ \text{perm.}\end{aligned} \tag{28}$$

3.1.1 Transverse galaxy bispectrum

As the full redshift space bispectrum is a complicated function of configurations described by five parameters (three parameters specifying triangle shape and two angles describing the orientation with respect to the line of sight), we will now simplify equation (28) by considering only triangles in the plane of the sky ($\mu_i = 0$), which are the easiest to model and are the triangles observed in photometric redshift surveys. In this case, we find a galaxy

bispectrum

$$B_{\rm g}^{\rm LA,\perp}(\boldsymbol{k}_1,\boldsymbol{k}_2,\boldsymbol{k}_3) = \left(b_1 - \frac{A_1}{3}\right)^2 \left[2\left(b_1 - \frac{A_1}{3}\right) F_2(\boldsymbol{k}_1,\boldsymbol{k}_2) + b_2 - \frac{2}{3}A_1 b_1\right] P(k_1)P(k_2) + 2\ \text{perm.} \tag{29}$$

Comparing this expression to equation (6), one finds that the effect of linear tidal alignments on the transverse galaxy bispectrum can be described as a rescaling of the galaxy bias parameters

$$b_1 \to b_1 - \frac{A_1}{3}, \quad b_2 \to b_2 - \frac{2}{3}A_1 b_1. \tag{30}$$

Hirata (2009) found that the same rescaling of b_1 applies to the real-space ($\mu_i = 0$) galaxy power spectrum. Therefore, *the use of the real-space power spectrum and bispectrum to eliminate galaxy bias parameters and extract σ_8 is robust against linear tidal alignments*. However, this robustness does not extend to the $\mu_i \neq 0$ modes.

For later use, we also write out the systematic error in the transverse galaxy bispectrum induced by linear alignment

$$\Delta B_{\rm g}^{\rm LA,\perp}(\boldsymbol{k}_1,\boldsymbol{k}_2,\boldsymbol{k}_3) = \left[2\left(b_1^2 A_1 - b_1\frac{A_1^2}{3} + \frac{A_1^3}{27}\right) F_2(\boldsymbol{k}_1,\boldsymbol{k}_2) - b_1\frac{A_1}{3}\right] P(k_1)P(k_2) + 2\ \text{perm.} \tag{31}$$

3.1.2 Normalization

Following Hirata (2009), we use $A_1 \approx -0.024$ for LRG-type elliptical galaxies. This is a rough estimate which is based on the assumption that elliptical galaxies are optically thin triaxial systems, that the deviation from spherical symmetry can on average be related to the tidal field (with correlation strength B), on different models for the orientation dependence of a galaxy's apparent magnitude (parametrized by χ), and the slope of the galaxy luminosity function η:

$$A_1 = 2\eta\chi B. \tag{32}$$

While the total flux of an optically thin galaxy is not affected by tidal alignments, the average isophotal ellipticity and projected effective radius of a galaxy become a function of the tidal field.

The selection of galaxies in a survey will be modified by tidal alignment if part of the selection criteria is a magnitude cut, and if the apparent magnitude of a galaxy depends on its orientation. The apparent magnitude of a galaxy is nearly orientation independent if measured using Petrosian magnitudes or model magnitudes which are based on an accurate model for the radial profile, then at the level of the toy model considered by Hirata (2009) $\epsilon \approx 0$.

If galaxies are selected using isophotal magnitudes or aperture magnitudes, more light will be counted if a galaxy is viewed along its long axis than its short axis. The selection factor χ in equation (32) depends on the method used to measure galaxy fluxes (cf. fig. 2 in Hirata 2009), and it translates the fractional change in effective radius induced by intrinsic alignment to a fractional change in measured flux. This change in measured flux moves galaxies across the selection threshold, and it is translated into change in number density by assuming a luminosity function with slope $-\eta$.

The strength of the tidal alignment effect B is determined from measurements of the density–ellipticity cross-correlation function (Hirata et al. 2007). Our chosen normalization further assumes an LRG luminosity function with $\eta = 4.0$ and galaxy selection based on isophotal magnitudes measured within $\sim$3 effective radii. Also note that this normalization is based on observations around $z = 0.3$ and should only be used near this redshift as the LRG luminosity function and the correlation between tidal field and galaxy orientation may show strong evolution with redshift.

3.2 Quadratic alignment

The leading-order alignment of galactic angular momentum in tidal torque theories is quadratic in the tidal tensor because of the need for both a tidal field and an anisotropic inertia tensor on which it can act.

The anisotropic selection function for a disc galaxy is generally a function of its inclination i (defined by $\cos i = \hat{\boldsymbol{L}}\cdot\hat{\boldsymbol{n}}$). While i is in the range $0 \le i \le \pi$, we expect most selection criteria to be symmetric with respect to an observer being above or below the plane of the target, so it follows that the anisotropic part of the selection function contains only even-order spherical harmonics:

$$\Upsilon(\mathbf{Q}\hat{\boldsymbol{n}},\boldsymbol{x}) = \sum_{J\ge 2,\ \text{even}} c_J P_J(\cos i), \tag{33}$$

where P_J is a Legendre polynomial. Using equation (17), and noting that for a disc galaxy, we may replace the general integration over orientations $\mathbf{Q} \in$SO(3) with an integration over directions of the angular momentum vector $\hat{\boldsymbol{L}} \in S^2$, we may write

$$\epsilon(\hat{\boldsymbol{n}}|\boldsymbol{x}) = \sum_{J\ge 2,\ \text{even}} c_J \int_{S^2} p(\hat{\boldsymbol{L}}|\boldsymbol{x}) P_J(\cos i)\,{\rm d}^2\hat{\boldsymbol{L}}. \tag{34}$$

Because the quadratic alignment model contains two factors of the tidal field, which are spin 2, $p(\hat{\boldsymbol{L}}|\boldsymbol{x})$ can contain spherical harmonics only through order $J \le 4$. For simplicity, we will focus only on the quadrupolar $J = 2$ term in the sum (while noting that the hexadecapolar alignment $J = 4$ is in principle possible). Then equation (34) implies that

$$\epsilon(\hat{\boldsymbol{n}}|\boldsymbol{x}) \propto \langle P_2(\hat{\boldsymbol{L}}\cdot\hat{\boldsymbol{n}})\rangle, \tag{35}$$

where the average is taken over the local probability distribution of $\hat{\boldsymbol{L}}$. Equivalently, using equation (15), we find that

$$\epsilon(\hat{\boldsymbol{n}}|\boldsymbol{x}) = \tilde{A}_2\left(\hat{n}_i\hat{n}_j - \frac{1}{3}\delta_{ij}\right)\hat{T}_{ih}\hat{T}_{hj}. \tag{36}$$

We relate $\hat{T}_{ij}$ to the dimensionless shear field tensor T_{ij},

$$\tilde{T}_{ij}(\boldsymbol{k}) = \frac{1}{4\pi G a^2\bar{\rho}_{\rm m}(a)}\left(k_i k_j - \frac{1}{3}\delta_{ij}k^2\right)\tilde{\Psi}(\boldsymbol{k}) = \left(\hat{k}_i\hat{k}_j - \frac{1}{3}\delta_{ij}\right)\tilde{\delta}(\boldsymbol{k}), \tag{37}$$

by approximating the scalar $T^2 \equiv T_{ij}T_{ji}$ with its expected value C^2:

$$C^2 \equiv \langle T^2\rangle = \frac{2}{3}\sigma^2(R), \tag{38}$$

i.e. we approximate $\hat{T}_{ij} \approx C^{-1}T_{ij}$. As this expression for the anisotropic selection function is already second order in the density field, effects associated with mapping ϵ to redshift space only enter at higher orders than considered in this analysis and in the following we will drop the superscript s to denote Fourier modes in redshift space.

Note that C^2 is proportional to the variance of the smoothed density field smoothed on the halo collapse scale R, since the density and tidal fields are both derived by taking second derivatives of the potential.

Then the contribution of quadratic alignment to the orientation-dependent selection function can be written as

$$\begin{aligned}\tilde{\epsilon}^{(2)}(\hat{\boldsymbol{n}}|\boldsymbol{k}) &= \tilde{A}_2\left(\hat{n}_i\hat{n}_j - \frac{1}{3}\delta_{ij}\right)\int\frac{\mathrm{d}^3\boldsymbol{k}'}{(2\pi)^3}\hat{\tilde{T}}_{ih}(\boldsymbol{k})\hat{\tilde{T}}_{hj}(\boldsymbol{k}'')\\ &= A_2\hat{n}_i\hat{n}_j\int\frac{\mathrm{d}^3\boldsymbol{k}'}{(2\pi)^3}\left\{\left(\hat{k}'_i\hat{k}'_h - \frac{1}{3}\delta_{ih}\right)\left(\hat{k}''_h\hat{k}''_j - \frac{1}{3}\delta_{hj}\right)\right.\\ &\quad\left. - \frac{1}{3}\delta_{ij}\left[(\hat{\boldsymbol{k}}'\cdot\hat{\boldsymbol{k}}'')^2 - \frac{1}{3}\right]\right\}\tilde{\delta}^{(1)}(\boldsymbol{k}')\tilde{\delta}^{(1)}(\boldsymbol{k}''),\end{aligned} \tag{39}$$

where $\boldsymbol{k}'' = \boldsymbol{k} - \boldsymbol{k}'$. This term contributes to the observed galaxy bispectrum via

$$\begin{aligned}\Delta B_{\rm g}^{\rm QA}(\boldsymbol{k}_1,\boldsymbol{k}_2,\boldsymbol{k}_3) &= 2A_2\left[b_1 - \frac{A_1}{3} + (A_1+f)\mu_1^2\right]\\ &\quad\times\left[b_1 - \frac{A_1}{3} + (A_1+f)\mu_2^2\right]P(k_1)P(k_2)\\ &\quad\times\left\{\mu_1\mu_2\hat{\boldsymbol{k}}_1\cdot\hat{\boldsymbol{k}}_2 - \frac{1}{3}\left[\mu_1^2+\mu_2^2+(\hat{\boldsymbol{k}}_1\cdot\hat{\boldsymbol{k}}_2)^2\right]\right.\\ &\quad\left.+\frac{2}{9}\right\} + 2\ \text{perm.}\end{aligned} \tag{40}$$

Here $A_1 \neq 0$ if the galaxy population under consideration is also subject to linear alignment, and we have defined $A_2 \equiv \tilde{A}_2/C^2$.

3.2.1 Transverse galaxy bispectrum

The quadratic alignment model modifies the observed transverse galaxy bispectrum by

$$\begin{aligned}\Delta B_{\rm g}^{\rm QA,\perp}(\boldsymbol{k}_1,\boldsymbol{k}_2,\boldsymbol{k}_3) &= \frac{2}{3}A_2b_1^2\left[\frac{2}{3} - \left(\hat{\boldsymbol{k}}_1\cdot\hat{\boldsymbol{k}}_2\right)^2\right]P(k_1)P(k_2)\\ &\quad + 2\ \text{perm.}\end{aligned} \tag{41}$$

Note that this systematic offset is independent of b_2, and its amplitude scales linearly with A_2 and quadratically with b_1. The systematic offset cannot be expressed as a simple rescaling of the galaxy bias parameters due to its shape dependence. Fig. 1 illustrates its effect on the reduced transverse galaxy bispectrum

$$Q_{\rm g}(\boldsymbol{k}_1,\boldsymbol{k}_2,\boldsymbol{k}_3) = \frac{B_{\rm g}(\boldsymbol{k}_1,\boldsymbol{k}_2,\boldsymbol{k}_3)}{P_{\rm g}(k_1)P_{\rm g}(k_2) + P_{\rm g}(k_1)P_{\rm g}(k_3) + P_{\rm g}(k_2)P_{\rm g}(k_3)}\ , \tag{42}$$

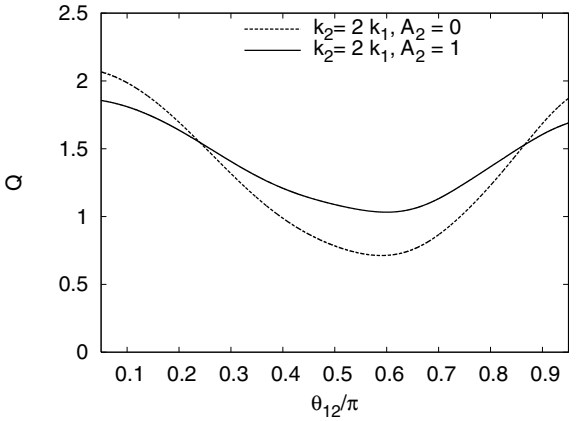

Figure 1. Effect of quadratic alignment on the reduced transverse galaxy bispectrum with $b_1 = 1, k_1 = 0.05h\,\mathrm{Mpc}^{-1}$, and where θ_{12} denotes the angle between $\boldsymbol{k}_1$ and $\boldsymbol{k}_2$, and for $A_2 = 1$.

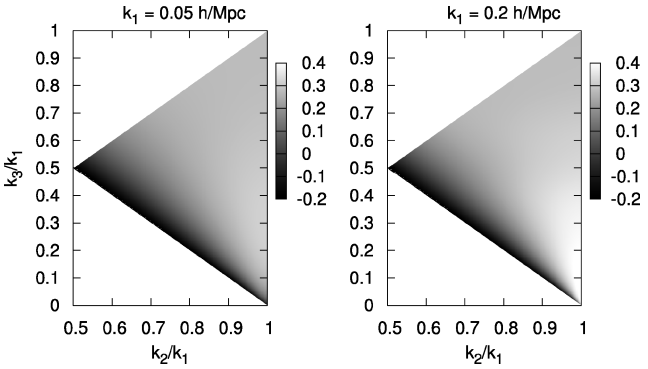

Figure 2. Systematic offset of the reduced transverse galaxy bispectrum due to quadratic alignment with $b_1 = 1$ and $A_2 = 1$ as a function of triangle shape and scale. Shown are all possible closed triangle configurations with $k_1 \geq k_2 \geq k3$ for a given k_1, areas in configuration space which do not correspond to a closed triangle are shown in white (located around the top and bottom left corner of each plot). Equilateral triangles are located in the upper right corner of the configuration space, isosceles triangles lie on the upper diagonal, and collinear ($\theta_{12} \to 0$) triangles near the lower diagonal.

which is only mildly dependent on cosmology as the amplitude of fluctuations has been divided out. The shape and scale dependence of $\Delta Q_{\rm g}$ is further illustrated in Fig. 2, which shows the systematic offset for all possible closed triangle configurations with $k_1 \geq k_2 \geq k3$, with the left plot showing triangles with $k_1 = 0.05h/\mathrm{Mpc}$ and the right plot showing triangles with $k_1 = 0.2h/\mathrm{Mpc}$. The systematic offset is negative for triangles which are close to collinear, and for the scales considered in this analysis it shows little scale dependence.

3.2.2 Normalization

Similar to the normalization of the linear alignment contamination outlined in Section 3.1.2, the magnitude of the observed contamination due to quadratic alignment again depends on (i) the orientation dependence of the recovered flux (continuum or line), (ii) the slope of the galaxy luminosity function and (iii) the strength of the tidal alignment effect. We may use models for (i) and direct measurements for (ii), but (iii) is harder. For the linear alignment model we were able to use the observational constraints from the density–ellipticity cross-correlation function, but this is not an option here as the quadratic alignment contribution to two-point statistics vanishes to leading order. Another option would be to set limits using the observed ellipticity variance, which must set an upper limit on α^2 (this was the approach followed in Crittenden et al. 2001 for estimating the intrinsic ellipticity correlation contamination of weak lensing surveys). We will take an even simpler approach here, and use some simple theoretical arguments on the value of α.

In the tidal torque model, the distribution of disc normal vectors $\hat{\boldsymbol{L}}$ given some tidal tensor $\hat{\mathbf{T}}$ can be approximated by (Crittenden et al. 2001)

$$p(\hat{\boldsymbol{L}}|\hat{\mathbf{T}}) \approx \frac{1}{4\pi}\left(1 + \frac{3\alpha}{2} - \frac{9\alpha}{2}\hat{L}_i\hat{L}_j\hat{T}_{ik}\hat{T}_{jk}\right). \tag{43}$$

For a geometrically thin disc with normal vector $\hat{\boldsymbol{L}}$ observed along the $\hat{z}$ axis, the inclination is $\cos i = \hat{L}_3$. The following constraints can be placed on α:

(i) Since $\hat{L}_i\hat{L}_j\hat{T}_{ik}\hat{T}_{jk}$ can take on any value between 0 and $\frac{2}{3}$, the requirement that $p(\hat{\boldsymbol{L}}|\hat{\mathbf{T}}) \geq 0$ sets the constraint $|\alpha| \leq \frac{2}{3}$.

(ii) If one neglects correlations between the external tidal field and the moment of inertia tensor of the collapsing protogalaxy, one finds $\alpha = \frac{3}{5}$ (Lee & Pen 2000).

(iii) The angular momentum of the disc of a galaxy may be disaligned from that of its host halo, due to e.g. torques between the disc and halo, or due to the disc containing only a specially selected subset of the halo's baryons. For a Gaussian distribution of disalingment angles with rms per axis Θ, the *JM* spherical harmonic component of $p(\hat{\boldsymbol{L}}|\hat{\mathbf{T}})$ is suppressed by a factor of exp $[-J(J+1)\Theta^2/2]$; since we have a quadrupolar anisotropy ($J = 2$), α is suppressed by a factor of exp $(-3\Theta^2)$.

The above arguments suggest that $|\alpha|$ of several tenths is plausible, but in no case should it exceed $\frac{2}{3}$. Also, while the simplest version of the tidal torque hypothesis implies $\alpha > 0$, there is no physical reason why negative values should not be allowed.

Next we determine the relation between an inclination-dependent observed flux and the selection function ϵ: Assume a galaxy flux distribution with slope $\mathrm{d}\ln\bar{n}/\mathrm{d}\ln F_{\rm min} = -\eta$. Then the number density of galaxies per logarithmic range in the intrinsic flux $F_{\rm i}$ per unit solid angle of disc orientation is

$$\mathcal{N}(F_{\rm i}, \hat{\boldsymbol{L}}) \propto F_{\rm i}^{-\eta} p(\hat{\boldsymbol{L}}|T). \tag{44}$$

Let the observed, inclination-dependent flux be $F(i) = F_{\rm i}\Phi(i)$. The number density of galaxies above some threshold flux F_0 then evaluates to

$$\begin{aligned}\mathcal{N}(>F_0) &\propto \int \mathrm{d}^2\hat{\boldsymbol{L}} \int_{F_0/\Phi(i)}^{\infty} \mathrm{d}\ln F_{\rm i} F_{\rm i}^{-\eta} p(\hat{\boldsymbol{L}}|\hat{\mathbf{T}}) \\ &\propto \int_0^{\pi} [\Phi(i)]^{\eta} \left[1 - \frac{9\alpha}{2}\left(\hat{T}_{3j}^2 - \frac{1}{3}\right) P_2[\cos(i)]\right] \sin i \ \mathrm{d}i,\end{aligned} \tag{45}$$

where we have performed both the integral over ϕ and over $F_{\rm i}$ (since the latter is simply a power law), and defined $\hat{T}_{3j}^2 \equiv \hat{T}_{3j}\hat{T}_{3j}$. Defining

$$\psi = \frac{\int_0^{\pi} [\Phi(i)]^{\eta} P_2(\cos i) \sin i \ \mathrm{d}i}{\int_0^{\pi} [\Phi(i)]^{\eta} \sin i \ \mathrm{d}i}, \tag{46}$$

the anisotropic part of the observed galaxy count can be written as

$$\epsilon(\hat{z}|\boldsymbol{x}) = -\frac{9\alpha}{2}\psi\left(\hat{T}_{3j}^2 - \frac{1}{3}\right). \tag{47}$$

Combining this with equation (36), we conclude that $\tilde{A}_2 = -\frac{9}{2}\alpha\psi$, and hence

$$A_2 = -\frac{9}{2}\frac{\alpha}{C^2}\psi = -\frac{27}{4}\frac{\alpha\psi}{\sigma_\delta^2(R)}. \tag{48}$$

The top-hat variance is related to the bias of the galaxies if the mass function is nearly universal (Sheth & Tormen 1999); for example, at $b = 1$ we have $\sigma_\delta^2(R) = 2.96$, whereas at $b = 2$ we have $\sigma_\delta^2(R) = 0.83$.

The last step in obtaining a numerical estimate for A_2 is evaluating the orientation-dependent selection factor ψ. This requires a model for the angular distribution of emitted radiance $\Phi(i)$, which also determines the selection probability $p(i) \propto [\Phi(i)]^{\eta}$. Several geometric toy models for the vertical distributions of emitters and dust are discussed by Hirata (2009), and for galaxy distributions with $\eta \approx 2$ (appropriate for [O II] and H_α surveys), ψ is found to be of the order of a few tenths: for example, it is $\psi = 0.4$ in the optically thick slab model; $\psi = 0.23$ (0.30) in the uniform slab model with normal optical depth $\tau = 0.5$ (1.0); and $\psi = 0.26$ (0.37) in the sheet-in-slab model with $\tau = 0.5$ (1.0).

These toy models suggest that A_2 will be of order unity and we assume $A_2 = 1$ for illustrative purpose in the following analysis.[1] For application to any survey the normalization must be calculated based on the detailed selection criteria and galaxy distribution.

4 FISHER MATRIX ANALYSIS

We now estimate the parameter bias induced by a tidal alignment contamination by performing a Fisher matrix analysis for a survey with characteristics similar to the Dark Energy Survey (DES),[2] assuming that one would use the angular bispectrum of a slice of galaxies in photometric redshift space. A spectroscopic survey covering a similar volume and oversampling the density field ($nP > 1$) would of course yield tighter constraints, but a full Fisher analysis of such a survey including redshift space distortions and Finger-of-God parameters is beyond the scope of this paper.

4.1 Survey characteristics and analysis details

Our fictitious survey has the same area as the DES, $\Omega = 5000\ \mathrm{deg}^2$. We assume a constant comoving galaxy density over the redshift range of interest and use a radial galaxy selection function of the form expected for the DES (Nock et al. 2010),

$$\frac{\mathrm{d\,Prob}}{dz} \propto \left(\frac{z}{0.5}\right)^2 \exp\left(-\frac{z}{0.5}\right)^{1.5}. \tag{49}$$

In order to project our redshift space distortions we consider the angular clustering of galaxies projected over a finite radial distance. For our theoretical modelling the projection over a finite range in radial distance is equivalent to a projection over a finite redshift range, and we choose $0.4 \le z \le 0.6$. Observationally, this mapping is complicated by the distribution of photometric redshifts and the effect of redshift space distortions on the boundary of a region selected in redshift space (e.g. Padmanabhan et al. 2007; Nock et al. 2010).

4.1.1 Binned angular multispectra and covariances

We calculate the angular power and multispectra $\mathcal{P}_N$ using the Limber equation in Fourier space (Kaiser 1992; Buchalter, Kamionkowski & Jaffe 2000):

$$\mathcal{P}_N(\boldsymbol{l}_1, \ldots, \boldsymbol{l}_N) = \int_{z=0.4}^{z=0.6} \mathrm{d}\chi \ \frac{\phi^N(\chi)}{\chi^{2N-2}} P_N\left(\frac{\boldsymbol{l}_1}{\chi}, \ldots, \frac{\boldsymbol{l}_N}{\chi}; \chi\right), \tag{50}$$

where P_N is the three-dimensional N-point correlation function in Fourier space. In the following we use $\mathcal{P}$, $\mathcal{B}$, $\mathcal{T}$ to denote the angular *galaxy* power spectrum, bispectrum and trispectrum.

For a linear alignment contamination, the change in the observed angular galaxy bispectrum is described by the same bias parameter rescaling (equation (30)) as for the transverse galaxy bispectrum discussed above. The magnitude of the systematic offset in the angular galaxy bispectrum induced by a quadratic alignment contamination is proportional to $A_2 b_1^2$ and independent of b_2. As the angular projection mixes different physical scales, the exact configuration dependence and normalization of the angular bispectrum contamination depends strongly on the radial selection function (for details see Fry & Thomas 1999). As can be seen from Fig. 2 the

[1] In principle, either *sign* of A_2 is allowed by our above calculations; for negative A_2 the direction of the parameter biases should be reversed.

[2] URL: http://www.darkenergysurvey.org/

systematic offset on the reduced transverse galaxy bispectrum is only weakly scale dependent, thus with our choice for the radial selection function the angular reduced bispectrum has very similar shape dependence.

The Limber approximation requires the transverse scales under consideration to be significantly smaller than the radial projection depth, hence we limit our analysis to angular scales corresponding to comoving Fourier modes $k \geq 0.04\ h\,\mathrm{Mpc}^{-1}$. As our intrinsic alignment toy models and biasing approximation are not designed to describe in the non-linear regime of structure formation, we will only consider angular frequencies corresponding to

$$0.04\ h\,\mathrm{Mpc}^{-1} \leq k \leq 0.2\ h\,\mathrm{Mpc}^{-1}. \tag{51}$$

We approximate the galaxy power spectrum by the linear matter power spectrum rescaled by the linear bias (equation (7)); bispectra and trispectra on these scales are approximated by the tree-level perturbation theory in combination with local biasing (equation (5)), i.e. using equations (7), (6) and (A4). These are evaluated using transfer functions generated by CMBFAST (Seljak & Zaldarriaga 1996) for the best-fitting *WMAP* 7 cosmology (Komatsu et al. 2010). Compared to an approach combining the halo model with halo occupation distribution modelling (e.g. Berlind & Weinberg 2002; Cooray & Sheth 2002) this is computationally much faster, the only model input is our biasing prescription and does not require halo models for intrinsic alignment. In the large-scale limits the halo models asymptote to the perturbation theory result, and at the scales of our analysis the galaxy power spectrum is fairly well described by perturbation theory (Cooray 2004; Smith, Sheth & Scoccimarro 2008). At redshift $z = 0$, Smith, Sheth & Scoccimarro (2008) find the reduced halo model bispectrum with $k_2 = 2k_1$ to be in close agreement with perturbation theory results at scales $k_1 \leq 0.1\ h/\mathrm{Mpc}$, except for collinear configuration ($\theta_{12} \to 0$). As we only consider triangle configurations with all angular frequencies $k_{1,2,3} \leq 0.2\,h\,\mathrm{Mpc}^{-1}$, the perturbation theory results should be sufficient at the level of this analysis. However, at scales smaller than $k \sim 0.1\ h/\mathrm{Mpc}$, Smith, Sheth & Scoccimarro 2008 and Guo & Jing (2009a) find the bispectrum measured from simulations to differ at the 10–20 per cent level from the perturbation theory. Note that these systematic effects on the determination of bias parameters on small scales are larger than the tidal alignment contaminations discussed here.

We model the observed power spectrum by averaging the angular power spectrum over bins of width $\Delta\, l$,

$$\mathcal{P}(\bar{l}) \equiv \int_{\bar{l}-1/2\Delta l}^{\bar{l}+1/2\Delta l} \frac{\mathrm{d}l\ l}{\bar{l}\Delta l}\mathcal{P}(l), \tag{52}$$

and the corresponding covariance is given by

$$\mathrm{Cov}[\mathcal{P}(\bar{l}_1)\mathcal{P}(\bar{l}_2)] = \frac{1}{\Omega}\left\{\delta_{\bar{l}_1,\bar{l}_2}\frac{4\pi}{\bar{l}_1\Delta l}\left[\mathcal{P}(\bar{l}_1)+\frac{1}{\bar{n}}\right]^2 \right. \tag{53}$$

$$\left. +\ \int_1\int_2 \mathcal{T}(\boldsymbol{l}_1, -\boldsymbol{l}_1, \boldsymbol{l}_2, -\boldsymbol{l}_2)\right\}, \tag{54}$$

where $\bar{n}$ is the average projected density of the galaxy population under consideration. Here the first term is a combination of Gaussian cosmic variance and shot noise. The second term involving the trispectrum of parallelogram configurations is the non-Gaussian power spectrum covariance.

The bispectrum is sampled with uniform binning $\Delta\, l$ in all angular frequencies. Defining

$$\int_i \equiv \int_{\bar{l}_i-1/2\Delta l}^{\bar{l}_i+1/2\Delta l} \frac{\mathrm{d}l_i\ l_i}{\bar{l}_i\Delta l}, \tag{55}$$

the bin-averaged bispectrum is given by

$$\mathcal{B}(\bar{l}_1,\bar{l}_2,\bar{l}_3) \equiv \int_1\int_2\int_3 \mathcal{B}(l_1,l_2,l_3)\delta_\mathrm{D}(\boldsymbol{l}_1+\boldsymbol{l}_2+\boldsymbol{l}_3). \tag{56}$$

We approximate the expression from Joachimi, Shi & Schneider (2009) for the full non-Gaussian covariance of the bin-averaged bispectrum by

$$\begin{aligned}
&\mathrm{Cov}[\mathcal{B}(\bar{l}_1,\bar{l}_2,\bar{l}_3)\mathcal{B}(\bar{l}_4,\bar{l}_5,\bar{l}_6)] \\
&= \frac{(2\pi)^3}{\Omega\bar{l}_1\bar{l}_2\bar{l}_3\Delta l^3}\Lambda^{-1}(\bar{l}_1,\bar{l}_2,\bar{l}_3) \\
&\quad\times D_{\bar{l}_1,\bar{l}_2,\bar{l}_3,\bar{l}_4,\bar{l}_5,\bar{l}_6}\left[\mathcal{P}(\bar{l}_1)+\frac{1}{\bar{n}}\right]\left[\mathcal{P}(\bar{l}_2)+\frac{1}{\bar{n}}\right]\left[\mathcal{P}(\bar{l}_3)+\frac{1}{\bar{n}}\right] \\
&\quad+\frac{2\pi\Lambda^{-1}(\bar{l}_1,\bar{l}_2,\bar{l}_3)\Lambda^{-1}(\bar{l}_4,\bar{l}_5,\bar{l}_6)}{\Omega}\delta_{\bar{l}_3,\bar{l}_4} \\
&\quad\times\int_1\int_2\int_3\int_5\int_6 \delta_\mathrm{D}(\boldsymbol{l}_1+\boldsymbol{l}_2+\boldsymbol{l}_3) \\
&\quad\times\{\delta_\mathrm{D}(\boldsymbol{l}_3+\boldsymbol{l}_5+\boldsymbol{l}_6)\,\mathcal{B}(l_1,l_2,l_3)\mathcal{B}(l_3,l_5,l_6) \\
&\quad+\delta_\mathrm{D}(-\boldsymbol{l}_3+\boldsymbol{l}_5+\boldsymbol{l}_6)\,\mathcal{T}(\boldsymbol{l}_1,\boldsymbol{l}_2,\boldsymbol{l}_5,\boldsymbol{l}_6)\mathcal{P}(l_3)\} + 8\ \mathrm{perm.},
\end{aligned} \tag{57}$$

where the symmetry factor $D_{\bar{l}_1\ldots\bar{l}_6}$ is non-zero only for diagonal elements of the covariance ($\{\bar{l}_1,\bar{l}_2,\bar{l}_3\} = \{\bar{l}_4,\bar{l}_5,\bar{l}_6\}$): $D_{\bar{l}_1\ldots\bar{l}_6} = 1$, 2 or 6 for scalene, isosceles or equilateral triangles, respectively. If $\bar{l}_1,\bar{l}_2,\bar{l}_3$ form a triangle, then $\Lambda^{-1}(\bar{l}_1,\bar{l}_2,\bar{l}_3)$ is the area of this triangle, otherwise $\Lambda^{-1} = 0$. The first term is the Gaussian (diagonal) part of the covariance which is proportional to the product of three power spectra which have been modified to account for Gaussian shot noise. The second/ third terms are non-Gaussian contributions from triangle pairs which have at least one common side so that the pentaspectrum can be factorized into two bispectra/ a trispectrum and a power spectrum. We have dropped a term which is proportional to the general connected pentaspectrum.

4.2 Biased parameter estimates for galaxy bias parameters

Having set up a model for the observable data and their covariances, we can now quantify the power of our fictitious survey at constraining model parameters using the Fisher matrix

$$\mathcal{F}_{\alpha\beta} = \frac{\partial\boldsymbol{\mathcal{P}}^t}{\partial p_\alpha}\mathrm{Cov}^{-1}(\boldsymbol{\mathcal{P}},\boldsymbol{\mathcal{P}})\frac{\partial\boldsymbol{\mathcal{P}}}{\partial p_\beta} + \frac{\partial\boldsymbol{\mathcal{B}}^t}{\partial p_\alpha}\mathrm{Cov}^{-1}(\boldsymbol{\mathcal{B}},\boldsymbol{\mathcal{B}})\frac{\partial\boldsymbol{\mathcal{B}}}{\partial p_\beta}, \tag{58}$$

where the $\boldsymbol{\mathcal{P}}$ and $\boldsymbol{\mathcal{B}}$ are data vectors with the binned angular *galaxy* power spectrum and bispectrum as data points. The data vectors and their covariances depend explicitly on the bias parameters through equations (7), (6) and (A4). Note that we do not include cross-correlations between power spectrum and bispectrum, both for simplicity and because they are small in the weakly non-linear regime (but see Sefusatti et al. 2006 for their constraining power in the weakly non-linear regime). The parameters of interest here are the linear and quadratic galaxy bias and we marginalize over the normalization of the matter power spectrum σ_8, i.e. $\boldsymbol{p} = (b_1, b_2, \sigma_8)$. Our fiducial model assumes $\sigma_8 = 0.8$, no intrinsic alignment contamination, and covers a range of bias parameters, while all other cosmological parameters are fixed to their best-fitting *WMAP* 7 values.

The inverse Fisher matrix serves as a lower limit on the marginalized covariance of statistical parameter errors

$$\langle\delta p_\alpha \delta p_\beta\rangle = (\mathcal{F}^{-1})_{\alpha\beta}\ . \tag{59}$$

Hence the statistical error on the inferred parameters is inversely proportional to $\sqrt{\Omega}$, as can be seen from the expressions (equations

54, 57) for the data covariances. The presence of a systematic error $\Delta\boldsymbol{\mathcal{B}}$, $\Delta\boldsymbol{\mathcal{P}}$ in the data which is not included in the model induces a bias in the parameter estimate compared to its fiducial values. To first order it is given by (e.g. Huterer et al. 2006; Amara & Réfrégier 2008):

$$\Delta p_\alpha = \langle \hat{p}_\alpha \rangle - p_\alpha^{\rm fid} = (\mathcal{F}^{-1})_{\alpha\beta} \left[\Delta\boldsymbol{\mathcal{P}}^t \, {\rm Cov}^{-1}(\boldsymbol{\mathcal{P}}, \boldsymbol{\mathcal{P}}) \frac{\partial \boldsymbol{\mathcal{P}}}{\partial p_\beta} + \Delta\boldsymbol{\mathcal{B}}^t \, {\rm Cov}^{-1}(\boldsymbol{\mathcal{B}}, \boldsymbol{\mathcal{B}}) \frac{\partial}{\boldsymbol{\mathcal{B}}} \partial p_\beta \right], \quad (60)$$

where the data vectors and covariances are evaluated at the fiducial model.

This systematic bias is independent of the survey area, but it is influenced by our choice of survey parameters through the selection function (equation 49) and data-binning scheme. It also depends on the projected number density of the galaxy population of interest as $\bar{n}$ determines the importance of shot noise. We adopt a uniform sampling with 20 equidistant bins in all angular frequencies (l_1, l_2, l_3) corresponding to equation (51) and assume a projected density of $\bar{n} = 1/\mathrm{arcmin}^2$ for a galaxy population in the redshift range $0.4 \leq z \leq 0.6$.

The systematic error on the bispectrum, $\Delta\boldsymbol{\mathcal{B}}$, due to linear or quadratic alignment is modelled by the line-of-sight projection (equation 50) of the tidal alignment contaminations (equations 29, 41) calculated in Section 3. We set $\Delta\boldsymbol{\mathcal{P}} = 0$ for the quadratic alignment model as the first correction to the power spectrum in the third order in the density contrast. In agreement with our findings from equation (30), the systematic error induced by linear alignment on the galaxy power spectrum is given by (cf. Hirata 2009)

$$\Delta P_{\rm g}^{\rm LA}(k_\perp) = \left[\left(b_1 - \frac{A_1}{3} \right)^2 - b_1^2 \right] P_{\rm g}(k_\perp), \quad (61)$$

where we have restricted $\boldsymbol{k}$ to be orthogonal to the line of sight as only these modes survive the Limber approximation.

Fig. 3 shows the marginalized Fisher matrix estimates of statistical parameter errors (95 per cent CL) obtained with our fictitious survey in the absence of an intrinsic alignment, and the systematic bias induced by a linear or quadratic alignment contamination.

The systematic bias induced by a linear alignment contamination (solid arrows) we find through the Fisher matrix analysis (equation 60) is in agreement with the analytic result (equation 30). The parameter bias on b_1 is independent of the value of b_2 assumed in the fiducial model and the solid arrows of different colour are indistinguishable. Assuming a normalization of $A_1 = -0.024$ as discussed in Section 3, the systematic error on b_2 is comparable to the 95 per cent CL statistical error for b_2 in our survey. The systematic error on b_1 caused by the linear alignment model is smaller, but may still be important if many photo-z slices are used in the parameter analysis. In the limit of our toy model, the effect of linear alignment on the angular galaxy power spectrum and bispectrum is fully described by a systematic error in the linear and non-linear bias parameter (equation 30) and it has no effect on measurements of σ_8.

The strength of the quadratic alignment contamination depends on triangle shape and size; it is *not* well described by a rescaling of the galaxy bias parameters. Hence the Fisher matrix estimates for the systematic parameter errors depend on the binning scheme and range of scales adopted in the analysis. For our choice of 20 equidistant bins per angular frequency, and with the range of scales being 0.04–0.2 h Mpc^{-1}, we observe a systematic shift towards larger non-linear bias b_2 and smaller b_1. The latter is degenerate between b_1 and σ_8. The plot illustrates a quadratic alignment contamination

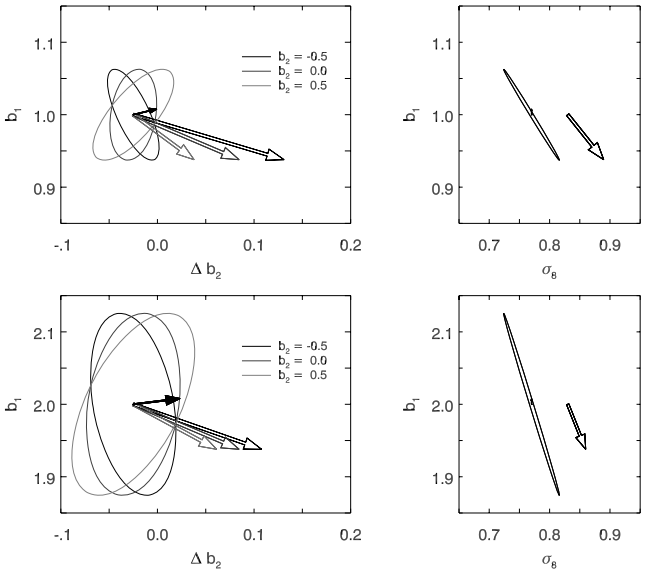

Figure 3. Systematic errors induced by intrinsic alignment. Ellipses show 95 per cent CL statistical errors on parameter estimates in a DES-like surveys for a fiducial model with $\sigma_8 = 0.8$, for a galaxy population with $b_1 = 1$ (top panels) or $b_1 = 2$ (bottom panel) and $b_2 \in \{-0.5, 0, 0.5\}$. Open/ filled arrows illustrate the systematic parameter shift induced by a quadratic/ linear intrinsic alignment contamination.

with normalization $A_2 = 1$. As can be seen from equations (41) and (60), the systematic bias is linear in A_2, and it reverses sign if $A_2 < 0$. While the exact form of the systematic error caused by the toy model for quadratic alignment depends on a number of parameters, it may cause a significant contamination in our fictitious survey if $|A_2| \gtrsim 0.5$, or if (as we expect) multiple photo-z slices are used to reduce statistical errors.

5 DISCUSSION

Using simple toy models for intrinsic alignment and the local bias approximation we have analyzed the effect of tidal alignment on the galaxy bispectrum. If the orientation of galaxies depends on the surrounding tidal field, and if the detection probability for galaxies is orientation dependent, the observed clustering of galaxies is modified by tidal alignments. This astrophysical contaminant can introduce systematic errors to parameters derived from the bispectrum.

A toy model for linear alignments (Catelan et al. 2001), which is based on the assumption that tidal fields elongate/compress haloes and thus determine galaxy shapes, results in a rescaling of linear and non-linear galaxy bias parameters that is proportional to the strength of the halo shape distortion. The presence of this systematic error in the observed galaxy bias measurements cannot be detected from projected clustering data as the strength of the alignment contamination is completely degenerate with the unobservable true bias parameters and outside information will be necessary to remove it. Normalizing the strength of the linear tidal alignment toy model to measurements of intrinsic alignments in weak lensing observations, we find that linear alignment may introduce systematic errors to galaxy bias measurements at the per cent level (again using only the real-space observables), and thus will likely not be significant.

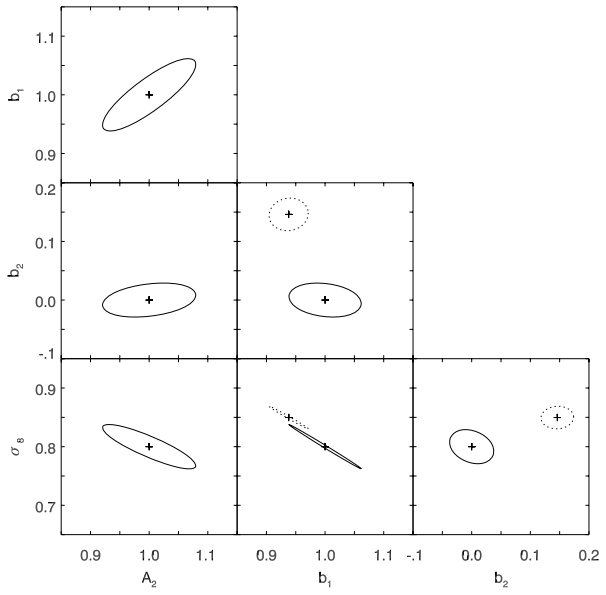

Figure 4. Removal of quadratic alignment bias. Dotted ellipses show the biased parameter estimates and their 95 per cent contour regions in the presence of quadratic alignment contamination with $A_2 = 1$ which is unaccounted for in the analysis. The solid ellipses illustrate the 95 per cent contour regions of the unbiased parameter estimates in an analysis which includes a quadratic alignment contamination and marginalizes over A_2.

Using a simple model for quadratic alignment based on galaxy spin correlations in linear tidal torque theory, we calculate a systematic contamination which modifies the shape of the galaxy bispectrum. Depending on survey characteristics, we find that quadratic alignment may introduce significant systematic errors to the galaxy bias parameters and the normalization of the power spectrum derived from the angular galaxy bispectrum. As the quadratic alignment contamination has different shape than the galaxy bispectrum, one can include a model for the contamination in the analysis and marginalize over its normalization. Fig. 4 illustrates how such a marginalization may remove the systematic bias at the cost of larger statistical errors. The biased data points and contour levels (dashed lines) are taken from Fig. 3 for a fiducial model with $b_1 = 1$ and $b_2 = 0$. The new statistical errors including marginalization over A_2 are calculated by adding A_2 as a nuisance parameter and including the contamination signal in the fiducial model of the Fisher matrix analysis ($\boldsymbol{\mathcal{B}} \rightarrow \boldsymbol{\mathcal{B}} + \Delta\boldsymbol{\mathcal{B}}$ in equation 58).

This analysis lives in the weakly non-linear regime to enable the use of simple models for linear and quadratic alignment. As the information content of the bispectrum increases dramatically with the maximal spatial frequency that is included in an analysis, any realistic analysis will have extent well into the quasi-linear regime. While models from the redshift space bispectrum on these scales (Smith et al. 2008) approach the required accuracy for such analyses, the treatment of tidal alignments including the non-Gaussian nature of the angular moment distribution and the non-linear stages of galaxy formation requires further work.

ACKNOWLEDGMENTS

EK and CMH are supported by the U.S. Department of Energy (DE-FG03-92-ER40701) and the National Science Foundation (AST-0807337). CMH is supported by the Alfred P. Sloan Foundation.

REFERENCES

Amara A., Réfrégier A., 2008, MNRAS, 391, 228
Berlind A. A., Weinberg D. H., 2002, ApJ, 575, 587
Bernardeau F., Colombi S., Gaztañaga E., Scoccimarro R., 2002, Phys. Rep., 367, 1
Binggeli B., 1982, A&A, 107, 338
Buchalter A., Kamionkowski M., Jaffe A. H., 2000, ApJ, 530, 36
Catelan P., Kamionkowski M., Blandford R. D., 2001, MNRAS, 320, L7
Cooray A., 2004, MNRAS, 348, 250
Cooray A., Sheth R., 2002, Phys. Rep., 372, 1
Crittenden R. G., Natarajan P., Pen U.-L., Theuns T., 2001, ApJ, 559, 552
Dolney D., Jain B., Takada M., 2006, MNRAS, 366, 884
Doroshkevich A. G., 1970, Astrophysics, 6, 320
Faltenbacher A., Li C., Mao S., van den Bosch F. C., Yang X., Jing Y. P., Pasquali A., Mo H. J., 2007, ApJ, 662, L71
Faltenbacher A., Li C., White S. D. M., Jing Y. P., Mao S., Wang J., 2009, Res. Astron. Astrophys., 9, 41
Feldman H. A., Frieman J. A., Fry J. N., Scoccimarro R., 2001, Phys. Rev. Lett., 86, 1434
Fry J. N., 1984, ApJ, 279, 499
Fry J. N., 1994, Phys. Rev. Lett., 73, 215
Fry J. N., Gaztañaga E., 1993, ApJ, 413, 447
Fry J. N., Thomas D., 1993, ApJ, 524, 591
Guo H., Jing Y. P., 2009a, ApJ, 698, 479
Guo H., Jing Y. P., 2009b, ApJ, 702, 425
Hatton S., Cole S., 1998, MNRAS, 296, 10
Heavens A. F., Matarrese S., Verde L., 1998, MNRAS, 301, 797
Hirata C. M., 2009, MNRAS, 399, 1074
Hirata C. M., Mandelbaum R., Ishak M., Seljak U., Nichol R., Pimbblet K. A., Ross N. P., Wake D., 2007, MNRAS, 381, 1197
Hoyle F., 1949, MNRAS, 109, 365
Hui L., Zhang J., 2008, ApJ, 688, 742
Huterer D., Takada M., Bernstein G., Jain B., 2006, MNRAS, 366, 101
Jackson J., 1972, MNRAS, 156, 1
Jing Y. P., Börner G., 2004, ApJ, 607, 140
Joachimi B., Shi X., Schneider P., 2009, A&A, 508, 1193
Kaiser N., 1984, ApJ, 284, L9
Kaiser N., 1987, MNRAS, 227, 1
Kaiser N., 1992, ApJ, 388, 272
Kayo I. et al., 2004, PASJ, 56, 415
Komatsu E. et al., 2010, ApJS, submitted (arXiv:1001.4538)
Kulkarni G. V., Nichol R. C., Sheth R. K., Seo H.-J., Eisenstein D. J., Gray A., 2007, MNRAS, 378, 1196
Lee J., Pen U.-L., 2000, ApJ, 532, L5
Lee J., Pen U.-L., 2007, ApJ, 670, 1
Mandelbaum R. et al., 2009, MNRAS, submitted (arXiv:0911.5347)
Manera M., Gaztañaga E., 2009, MNRAS, submitted (arXiv:0912.0446)
Marín F. A., Wechsler R. H., Frieman J. A., Nichol R. C., 2008, ApJ, 672, 849
McDonald P., 2006, Phys. Rev. D, 74, 103512
McDonald P., Roy A., 2009, J. Cosmol. Astropart. Phys., 08, 020
Nichol R. C. et al., 2006, MNRAS, 368, 1507
Niederste-Ostholt M., Strauss M. A., Dong F., Koester B., McKay T. A., 2010, MNRAS, 405, 2023
Nock K., Percival W. J., Ross A. J., 2010, MNRAS, 407, 520
Padmanabhan N. et al., 2007, MNRAS, 378, 852
Peacock J. et al., 2001, Nat, 410, 169
Peebles P. J. E., 1969, ApJ, 155, 393
Reid B. A., Spergel D. N., Bode P., 2009, ApJ, 702, 249
Schäfer B. M., 2009, Int. J. Mod. Phys. D, 18, 173
Sciama D., 1955, MNRAS, 115, 3
Scoccimarro R., Couchman H. M. P., Frieman J. A., 1999, ApJ, 517, 531
Scoccimarro R., Feldman H. A., Fry J. N., Frieman J. A., 2001, ApJ, 546, 652
Sefusatti E., Crocce M., Pueblas S., Scoccimarro R., 2006, Phys. Rev. D, 74, 023522
Seljak U., 2000, MNRAS, 318, 203

Seljak U., Zaldarriaga M., 1996, ApJ, 469, 437
Sheth R., Tormen G., 1999, MNRAS, 308, 119
Smith R. E., Sheth R. K., Scoccimarro R., 2008, Phys. Rev. D, 78, 023523
Tegmark M. et al., 2004, ApJ, 606, 702
van den Bosch F., Abel T., Croft R., Hernquist L., White S. D. M., 2002, ApJ, 576, 21
Verde L., Heavens A., Matarrese S., Moscardini L., 1998, MNRAS, 300, 747
Verde L., Heavens A., Matarrese S., 2000, MNRAS, 318, 584
Verde L. et al., 2002, MNRAS, 335, 432
White S. D. M., 1984, ApJ, 286, 38

APPENDIX A: TREE-LEVEL GALAXY TRISPECTRUM

To calculate the tree-level matter trispectrum we need to consider the density contrast to third order as the tree-level trispectrum splits into two types of connected terms, $\langle\tilde{\delta}^{(1)}\tilde{\delta}^{(1)}\tilde{\delta}^{(2)}\tilde{\delta}^{(2)}\rangle_{\rm c}$ and $\langle\tilde{\delta}^{(1)}\tilde{\delta}^{(1)}\tilde{\delta}^{(1)}\tilde{\delta}^{(3)}\rangle_{\rm c}$. The third-order density contrast is given by (Fry 1984)

$$\tilde{\delta}^{(3)}(\boldsymbol{k}) = \int \frac{{\rm d}^3\boldsymbol{k}_1}{(2\pi)^3}\int \frac{{\rm d}^3\boldsymbol{k}_2}{(2\pi)^3} F_3\left(\boldsymbol{k}_1, \boldsymbol{k}_2, \boldsymbol{k}-\boldsymbol{k}_1-\boldsymbol{k}_2\right) \times \tilde{\delta}^{(1)}(\boldsymbol{k}_1)\tilde{\delta}^{(1)}(\boldsymbol{k}_2)\tilde{\delta}^{(1)}(\boldsymbol{k}-\boldsymbol{k}_1-\boldsymbol{k}_2), \tag{A1}$$

with the third-order coupling function F_3. One finds for the matter trispectrum

$$\begin{aligned}(2\pi)^3\delta_{\rm D}(\boldsymbol{k}_{1234})T_{\rm pt}(\boldsymbol{k}_1,\boldsymbol{k}_2,\boldsymbol{k}_3,\boldsymbol{k}_4) &\approx \left\langle\tilde{\delta}^{(1)}(\boldsymbol{k}_1)\tilde{\delta}^{(1)}(\boldsymbol{k}_2)\tilde{\delta}^{(1)}(\boldsymbol{k}_3)\tilde{\delta}^{(3)}(\boldsymbol{k}_4)\right\rangle + 3\ \text{perm.} \\ &+ \left\langle\tilde{\delta}^{(1)}(\boldsymbol{k}_1)\tilde{\delta}^{(1)}(\boldsymbol{k}_2)\tilde{\delta}^{(2)}(\boldsymbol{k}_3)\tilde{\delta}^{(2)}(\boldsymbol{k}_4)\right\rangle + 5\ \text{perm.}\end{aligned} \tag{A2}$$

After some algebra one obtains

$$\begin{aligned}T_{\rm pt}(\boldsymbol{k}_1,\boldsymbol{k}_2,\boldsymbol{k}_3,\boldsymbol{k}_4) &= 6F_3^{\rm s}(\boldsymbol{k}_1,\boldsymbol{k}_2,\boldsymbol{k}_3)P(k_1)P(k_2)P(k_3) + 3\ \text{perm.} \\ &+ 4[P(k_{13})F_2(\boldsymbol{k}_1,-\boldsymbol{k}_{13})F_2(\boldsymbol{k}_2,\boldsymbol{k}_{13}) \\ &+ P(k_{23})F_2(\boldsymbol{k}_1,\boldsymbol{k}_{23})F_2(\boldsymbol{k}_2,-\boldsymbol{k}_{23})] \\ &\times P(k_1)P(k_2) + 5\ \text{perm.}\end{aligned} \tag{A3}$$

If one assume the third-order galaxy bias (b_3) to be zero, two types of additional terms containing the quadratic galaxy bias contribute to the galaxy trispectrum, $\langle b_1\tilde{\delta}^{(1)}\, b_1\tilde{\delta}^{(1)}\, b_1\tilde{\delta}^{(2)}\, b_2\tilde{\delta}^{(1)}\otimes\tilde{\delta}^{(1)}\rangle_{\rm c}$ and $\langle b_1\tilde{\delta}^{(1)}\, b_1\tilde{\delta}^{(1)}\, b_2\tilde{\delta}^{(1)}\otimes\tilde{\delta}^{(1)}\, b_2\tilde{\delta}^{(1)}\otimes\tilde{\delta}^{(1)}\rangle_{\rm c}$. Hence our model for the galaxy trispectrum is given by

$$\begin{aligned}T_{\rm gal}(\boldsymbol{k}_1,\boldsymbol{k}_2,\boldsymbol{k}_3,\boldsymbol{k}_4) &\approx b_1^4 T_{\rm pt}(\boldsymbol{k}_1,\boldsymbol{k}_2,\boldsymbol{k}_3,\boldsymbol{k}_4) \\ &+ 2b_1^3 b_2 P(k_1)P(k_2)[P(k_{13})F_2(\boldsymbol{k}_1,-\boldsymbol{k}_{13}) \\ &+ P(k_{24})F_2(\boldsymbol{k}_2,-\boldsymbol{k}_{23})] + 5\ \text{perm.} \\ &+ 4b_1^2 b_2^2 P(k_1)P(k_2)\,[P(k_{13})+P(k_{23})] \\ &+ 5\ \text{perm.}\end{aligned} \tag{A4}$$

This paper has been typeset from a TEX/LATEX file prepared by the author.